Computational Materials Science 122 (2016) 281–287

Contents lists available at ScienceDirect

Computational Materials Science

journal homepage: www.elsevier.com/locate/commatsci

An efficient computational technique for modeling dislocation–precipitate interactions within dislocation dynamics

Amirreza Keyhani [a], Reza Roumina [b,*], Soheil Mohammadi [a]

[a] High Performance Computing Lab (HPC), School of Civil Engineering, College of Engineering, University of Tehran, Tehran, Iran
[b] School of Metallurgical and Materials Engineering, College of Engineering, University of Tehran, Tehran, Iran

ARTICLE INFO

Article history:
Received 19 February 2016
Received in revised form 8 May 2016
Accepted 27 May 2016

Keywords:
Dislocation dynamics (DD)
Shearable and non-shearable precipitates
Dislocation–precipitate interaction

ABSTRACT

A new computational technique for modeling dislocation interactions with shearable and non-shearable precipitates within the line dislocation dynamics framework is presented. While shearable precipitates are modeled by defining a resistance function, non-shearable ones are modeled by drawing a comparison between the two well-known Orowan and Frank–Read mechanisms. The precipitates are modeled directly within the dislocation dynamics analysis without the need for any additional numerical methods. Due to low computational cost the method is appropriate for simulation of a high dislocation density interacting with large number of precipitates considering different types and various sizes and resistances. It is also efficient for coupling dislocation dynamics with finite element method in multi-scale frameworks since it does not require the mesh to be consistent with the precipitates geometry.

1. Introduction

Computational approaches to study dislocation–precipitate interaction, commenced from 60s, have provided more insight in understanding plasticity of metals and alloys [1]. A comprehensive review of classical simulation methods can be found in [2]. Since the advent of the dislocation dynamics (DD), which is a computational framework to analyze dislocation motions and their related phenomena at micron scale [3–7], some attempts have been made to study dislocation interactions with precipitates and boundaries within the dislocation dynamics analysis [8–10]. For a comprehensive review of advances in dislocation dynamics modeling, see [11].

Modeling precipitates in dislocation dynamics analysis was generally limited to specific assumptions for the stress fields arising from precipitates. In some studies, precipitates were introduced as spherical stress fields [12–18], while some others evaluated the stress field due to matrix and precipitate shear modulus difference by applying the superposition principle, in which the problem was disintegrated into two problems: an infinite domain containing dislocations and a correction problem for considering the elastic field of precipitate and treating the boundary conditions. As a result, an extra numerical method, such as FEM or BEM, was required for analysis of the second part [19–21]. The stress fields due to lattice misfit at internal boundaries were taken into account in a few studies or by coupling DD with FEM [12,22] or with the fast Fourier transform (FFT) [23].

The abovementioned approaches suffer from one or several flaws in terms of physics or disadvantages with reference to computational cost or both. First, the effect of misfit dislocations was not considered in some methodologies, though it had a significant role in dislocation–precipitate interaction. For instance, a dislocation could pass a precipitate with the similar shear modulus of matrix without any interactions. This was in contrast with real problems where dislocations might stop behind the precipitate or hardly pass through it because of misfit dislocations at the coherent precipitate–metal matrix interface. Second, due to the high stress gradient near precipitates, considerable time was required to obtain a converged solution for the dislocation motion near precipitates. Third, even after forming the Orowan loops, the associated nodes still remained in the mobility equations, increasing the computational effort required to solve the mobility equations at each time step. Finally, an extra numerical method such as FEM, BEM or FFT was required to analyze the stress field of a precipitate. In a number of studies [12–18], the extra numerical method was avoided by defining precipitates as spherical stress fields; however, the first three disadvantages remained unsolved.

In the present study, a computational technique is proposed to model precipitates with various sizes and resistances within the line dislocation dynamics analysis which eliminates the mentioned drawbacks. The developed method is also efficient for modeling

* Corresponding author.
E-mail addresses: amir.keyhani@ut.ac.ir (A. Keyhani), roumina@ut.ac.ir (R. Roumina), smoham@ut.ac.ir (S. Mohammadi).

http://dx.doi.org/10.1016/j.commatsci.2016.05.036
0927-0256/

precipitates in a combined FEM-DD framework to address plastic deformations in small scales. Implementation of this technique in FEM-DD framework allows for the independency of mesh generation from the precipitates geometry, which simplifies the solution of large systems with random distribution of precipitates by adopting very simple mesh generations, less degrees of freedom (DOFs) and low computational costs.

2. Modeling approach

In this study, a modified version of line dislocation dynamics (DD) simulation code, DDLab, is adopted to model dislocation motions [24]. In dislocation dynamics simulations, a dislocation curve is discretized into straight segments defined by two end nodes. The mobility function $\mathbf{M}$ relates the vector of nodal forces $\mathbf{f}_i$ to the nodal velocities $\mathbf{v}_i$,

$$\mathbf{v}_i = \mathbf{M}(\mathbf{f}_i) \tag{1}$$

The velocity of the node i, $\mathbf{v}_i$, also relies on the forces acting on the other nodes. The dislocation segment orientation and material properties are the main influential factors on the mobility function. In the dislocation dynamics procedure, the nodal velocity is calculated by solving the mobility equations and the dislocation motion is computed via topological considerations [25].

When a dislocation encounters a precipitate, it bends so the related shear stress which the dislocation exerts on a precipitate increases. If this stress reaches a critical value, the dislocation goes on the verge of passing the precipitate. At this point, the dislocation can pass the precipitate by two mechanisms relying on the precipitate resistance, τ_{obs}, which is defined as the minimum required shear stress to cut a precipitate. First, the dislocation rounds the precipitate (the Orowan mechanism) unless the arising stress from the dislocation bending overcomes the precipitate resistance. Second, the dislocation cuts through the precipitates if the precipitate resistance is lower than the induced stress due to the dislocation bending. It is worth emphasizing that the applied stress to the dislocation must be large enough to bend the dislocation to a critical state in order to pass a precipitate.

To model the first mechanism (non-shearable precipitates), it is considered that a dislocation node which locates closer than a specific distance to a precipitate gets locked, as depicted in Fig. 1. By this approach, the main problem of dislocation–precipitate interaction is transformed into the Frank–Read mechanism, since the dislocation line pinned between two precipitates behaves similar to a Frank–Read source. The critical resolved shear stress (CRSS) obtained from the Frank–Read and the Orowan mechanisms depends on the maximum dislocation line curvature and the material properties. Therefore, for an identical material, the two mechanisms predict the equal CRSS for a given dislocation line curvature. Assuming a constant curvature along the bowing dislocation line results in $\tau_{nuc} = \mu b / L_f$, where μ is the shear modulus, b is the magnitude of the Burgers vector and L_f is the length of the initial dislocation line. If the anisotropic line tension is considered, the dislocation line at the critical state will have an oval shape [26]. The critical stress is expressed in a general form $\tau_{nuc} = \beta \mu b / L_f$ by adopting the concept of self-stress [27] to investigate the bowing of dislocation line [28]. The constant β depends on the Poisson's ratio, the dislocation core radius and the dislocation line properties.

For the critical stress of two mechanisms to be equal, it is assumed that a dislocation rounds a precipitate with a modeling diameter D_1, which is not equal to the precipitate diameter D. Having equivalent Frank–Read nucleation stress and Orowan stress $\tau_{Orowan} = \mu b \ln(\bar{D}/r_0)/(2\pi L)$, the modeling diameter of a precipitate can now be determined (see Fig. 1):

$$L_f = L + D - D_1 \tag{2}$$

$$D_1 = L + D - 2\pi L \beta \left[\ln\left(\bar{D}/r_0\right)\right]^{-1} \tag{3}$$

where L is the internal distance between the two precipitates, r_0 is the core radius of dislocation and $\bar{D} = \left(D^{-1} + L^{-1}\right)^{-1}$.

The maximum stress that a dislocation can exert on a precipitate occurs when the dislocation radius of curvature equals the modeling radius, $\tau_{max} = \mu b / D_1$. Whenever the precipitate resistance reaches to this magnitude (i.e. $\tau_{obs} = \tau_{max}$), the dislocation stops behind the precipitate completely, representing the Orowan regime. If the precipitate resistance is lower than the maximum stress (i.e. $\tau_{obs} < \tau_{max}$), the dislocation can pass the precipitate by exerting a lower level of stress to the precipitate, which generates a radius of curvature larger than the modeling radius.

To keep up with the second mechanism (i.e. shearable precipitates), the precipitate resistance scale, $R = \tau_{obs}/\tau_{max}$, is defined; which is set to 1 for a non-shearable precipitate and 0 when no precipitate exists. When the distance of a node from the center of a precipitate is less than the modeling radius, the node gets locked in the dislocation dynamics procedure. At each step, the local shear stress, which is related to the local curvature at this point, is compared with the precipitate resistance. If the related local shear stress exceeds the precipitate resistance, the node is released.

The precipitate resistance arises from several factors including the matrix and precipitate shear modulus difference, misfit dislocations and strains and the dislocation core energy change due to the difference between crystalline structures of matrix and precipitates. While the first factor is usually considered in modeling precipitates in dislocation dynamics, the second and third ones have a controlling effect. Small scale analyses are required to determine the precipitate resistance in a matrix. Some attempts have been made to introduce the critical resolved shear stress, τ_c, as a function of shear modulus difference between the

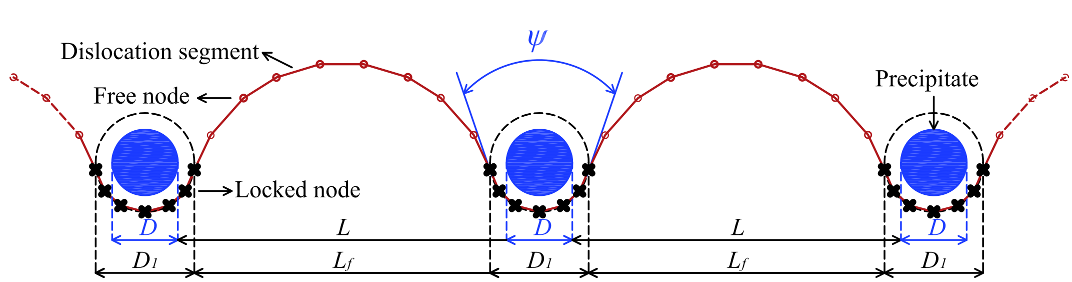

Fig. 1. Nodes which are positioned closer than a specific distance to the precipitate get locked. The circles and crosses represent the free and locked nodes, respectively. A dislocation line between two precipitates with the internal distance L acts as a Frank–Read source with length L_f. ψ is the angle between the dislocation tangents at both sides of the precipitate.

matrix and precipitates [20,29]. The results of these analyses can be utilized in the present technique to determine R.

Writing the equilibrium at the critical state,

$$\tau_c L_f = \tau_{\mathrm{obs}} D_1 \tag{4}$$

and substituting $\tau_{\mathrm{obs}} = R\tau_{\max}$ and $\tau_{\max} = \mu b/D_1$ results in

$$R = \tau_c/\tau_0 \tag{5}$$

where $\tau_0 = \mu b/L_f$. According to [20,29], R is a function of $\xi = \mu_p/\mu_m$ and $\eta = r_p/b$ where μ_p and μ_m are precipitate and matrix shear modulus, respectively and r_p is the precipitate radius. For large values of ξ, R slightly depends on L. Section 3.1 presents the way R is calculated for a specific problem [20].

The key concept in handling the physics of dislocation–precipitate interaction is to redefine critical stress required for moving a dislocation through a distribution of precipitates. In order to verify this methodology, the ratio of the CRSS considering the anisotropic line tension to the CRSS assuming the isotropic line tension, τ_c^*, and the breaking angle ψ for various precipitates resistances are calculated by dislocation dynamics simulations and compared with the benchmark results [30–32] in Fig. 2, which clearly shows a good agreement. Two crystalline structures are considered; (1) an FCC Cu crystal with the shear modulus of $G = 63.2$ GPa and the Poisson's ratio of $\upsilon = 0.305$, (2) a BCC Fe crystal with the shear modulus of $G = 81$ GPa and the Poisson's ratio of $\upsilon = 0.29$. The Burgers vector in the Cu crystal is considered as $\mathbf{b} = [0.181 \quad 0.181 \quad 0]$ nm with the glide plane of $(\bar{1}\ 1\ 1)$ and for the Fe crystal, the Burgers vector and the glide plane are $\mathbf{b} = [0.143 \quad 0.143 \quad 0.143]$ nm and $(\bar{1}\ 0\ 1)$, respectively.

There is a difference between the theoretical values and those generated by the reference computer simulations for small values of ψ_c [2]. It arises from the fact that due to the assumption of a constant line tension along the dislocation, its geometry has to be a circular shape. However, on the release point the dislocation line becomes semicircular between the two precipitates. In the present simulations, the anisotropic line tension and the possible Orowan loop around a single precipitate is considered. Setting $\beta = 1$ in Eq. (3), the simulation results converge to the theoretical values of the isotropic line tension assumption. For $\beta = 0.75$ [31,32], the results converge to the benchmark studies based on the assumption of anisotropic line tension.

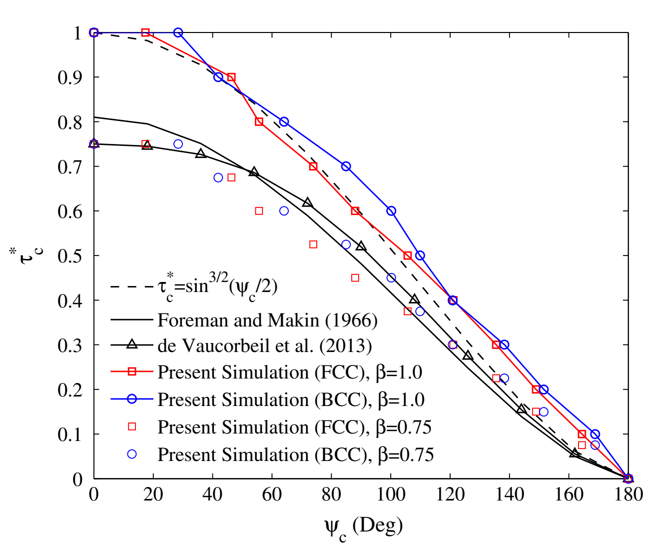

Fig. 2. The critical stress versus the bypass angle. Comparison of the present results with the reference results [2,30–32].

The present methodology is also capable of handling shearable to non-shearable transition of precipitates as the diameter of the precipitates increases. By increasing the diameter of a precipitate, the local curvature of the dislocation line adjacent to the precipitate decreases. Consequently, the maximum shear stress that the dislocation line applies to the precipitate decreases ($\tau_{\max} = \mu b/D_1$). If the diameter of the precipitate reaches to a certain value, D_1^c, the resulting shear stress due to dislocation line curvature near the precipitate is not large enough to cut the precipitate. Therefore, the dislocation line overpasses the precipitate. Substituting $\tau_{\mathrm{obs}} = R\tau_{\max}$ and $\tau_{\max} = \mu b/D_1$ in the equilibrium equation at the critical state leads to,

$$R = \frac{\tau_{\mathrm{obs}} D_1}{\mu b} \tag{6}$$

which shows that R increases by increasing the diameter of the precipitate. The critical diameter of precipitate, D_1^c, can be calculated by equating R to unity, meaning that the Orowan loop forms around the precipitate,

$$D_1^c = \frac{\mu b}{\tau_{\mathrm{obs}}} \tag{7}$$

If movements of dislocations continue, many dislocation lines may encounter a precipitate and lead to form numerous Orowan loops around a non-shearable precipitate. Consequently, the flow stress increases due to two major reasons. First, forming each Orowan loop increases the back stress which arises from the precipitate and loops. Second, the accumulated Orowan loops decrease the length of the Frank–Read source forming between two precipitates, known as the source shortening effect [33,34].

The present technique can be extended to handle further Orowan loops around a precipitate by a similar approach used to model the first one. To calculate the diameter of the n-th loop, D_n can be determined from

$$\tau_c|_{D=D_n} = \tau_c|_{D=D_1} + \tau_h^n, \tag{8}$$

τ_h^n is the amount of increase in hardening stress due to forming n loops around a precipitate [19,35],

$$\tau_h^n = ncb\mu_m \left(1 - \frac{\upsilon}{2(1-\upsilon)}\right) \frac{D^2}{4(L+D)^3} \tag{9}$$

where c is a geometrical parameter. Substituting Eq. (9) in (8) and considering $\tau_{cr} = \beta\mu b/(L - D_n)$,

$$D_n = L + D - \left[c(n-1)\left(1 - \frac{\upsilon}{2(1-\upsilon)}\right)\frac{D^2}{4(L+D)^3} + \frac{1}{L+D-D_1}\right]^{-1} \tag{10}$$

For infinite loops, D_n approaches to $L + D$, which means that the modeling precipitate diameter becomes equal to center-to-center distance of precipitates.

The mentioned disadvantages of former methods are clearly eliminated by the present modeling approach. First, the effect of misfit dislocations can be indirectly considered in the precipitate resistance. Second, the converged solutions around precipitates are obtained faster since this methodology does not involve any high stress gradient near precipitates. Third, the locking nodes, which are positioned inside the modeling radius, are omitted from the mobility equations. Therefore, the number of mobility equations and computational costs are decreased. It should be noted that although the locked nodes are omitted from the mobility equations, their associated stress fields are considered. Finally, both types of precipitates are modeled directly within the line dislocation dynamics analysis without requiring any additional numerical methods.

3. Results and discussion

Three different problems of dislocation–precipitate interaction are simulated by utilizing the present method to show its accuracy and efficiency. In Section 3.1, the effect of precipitate to matrix shear modulus ratio on strength is studied in an Fe crystal and the hardening stress due to forming further Orowan loops around precipitates is investigated in Section 3.2. Finally, the analysis of plastic deformation in a micro cuboid, which contains a density of dislocations with various precipitate sizes, is performed in a coupled FEM-DD framework in Section 3.3.

3.1. The effect of precipitate to matrix shear modulus ratio on strength

The effect of precipitate to matrix shear modulus ratio on the strength of an Fe crystal is investigated. The properties of the Fe crystal are similar to the former section. In this simulation R is determined on the basis of precipitate to matrix shear modulus ratio. The presented results for this problem [20] are fitted by the following function,

$$R(\xi,\eta)=\begin{cases}(\xi-1)(a_1\eta-a_2) & \xi\leqslant 1\\ 1+\frac{1}{a_3\xi^2+a_4\xi^2\eta^2+a_5\xi^2+a_6} & \xi>1\end{cases}\tag{11}$$

which is valid under some special conditions. First, it must be equal to zero when $\xi = 1$, since there is no additional resistance to dislocation glide. In addition, as ξ or η approaches to infinity, R must approach to 1, which represents a non-shearable precipitate. Therefore, a resistance function is generally similar to Eq. (11); however, the coefficients a_1–a_5 are adjustable for different problems. The coefficients of the resistance function, Eq. (11), for the considered problem are calculated by curve fitting of the results by [20] and they are presented in Table 1. The corresponding resistance function is plotted in Fig. 3.

Although the locking distance is not explicitly derived from the image stress due to matrix and precipitate shear modulus difference, the resulting image stress due to shear modulus difference is embedded in the proposed methodology. The locking distance for non-shearable precipitates is derived based on the Orowan mechanism in which the μ_p/μ_m is relatively high and for shearable precipitates, the dislocation nodes get locked and unlocked based on the resistance function which is related to the shear modulus ratio (μ_p/μ_m).

The normalized critical resolved shear stress (τ_c/τ_0) versus precipitate and matrix shear modulus ratio (μ_p/μ_m) for a dislocation line encountering a line array of 10 nm diameter precipitates is presented in Fig. 4, which shows a good agreement with the reference results [20]. It is worth to emphasize that the proposed resistance scale function, Eq. (11), is calculated only by considering precipitate and matrix shear modulus difference and other factors are not taken into account. In order to assess the effects of other determining factors such as misfit dislocations and strains, independent analyses should be performed to allow for more accurate definition of the resistance scale function.

Table 1
The coefficients of Eq. (11) for the considered problem.

a_1	a_2	a_3	a_4	a_5	a_6
−0.0068	−0.2458	0.8278	−0.1315	0.1308	−1.8173

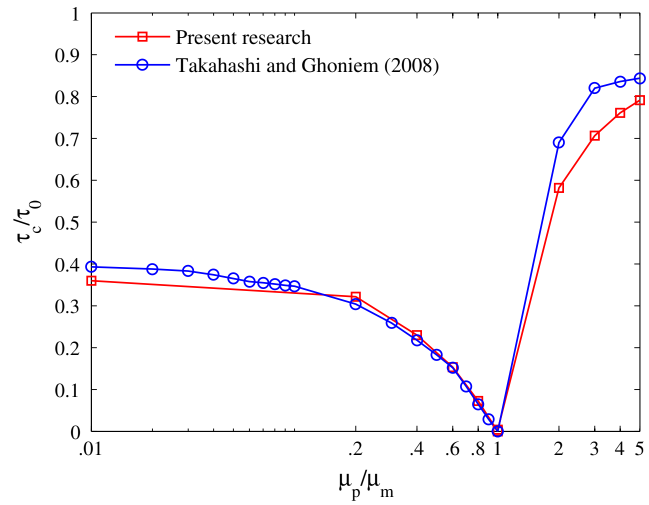

Fig. 4. Normalized critical resolved shear stress versus precipitate to matrix shear modulus ratio [20].

3.2. The hardening stress due to forming n loops around precipitates

The diameter of n-th loop around a non-shearable precipitate with the diameter of 0.1 μm and center-to-center spacing of 0.6 μm in an Fe crystal with the same mechanical properties as before is calculated from Eq. (10) and compared with the results of dislocation dynamics simulations presented in [36], Fig. 5(a). According to [36], the value of 35 was found for c. The diameter of n-th loop, Eq. (10), is assigned to each precipitate in dislocation dynamics simulations and the resulting hardening stress due to forming n loops around precipitates is compared with [36] in Fig. 5, which shows a reasonable agreement. The geometry of dislocation line at the critical state for n = 1, 2, 3 and 4 are presented in Fig. 6. Fig. 6 illustrates that the formation of each loop decreases the precipitate spacing, which increases the curvature of the dislocation line. The increase in maximum curvature causes the increase in critical stress, Fig. 5(b).

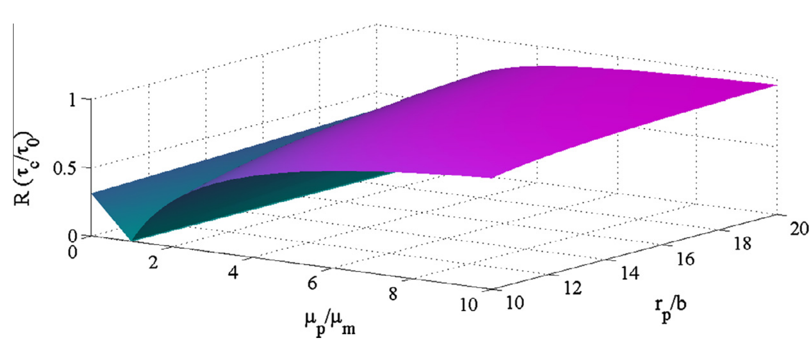

Fig. 3. Typical resistance of precipitates as a function of μ_p/μ_m and r_p/b.

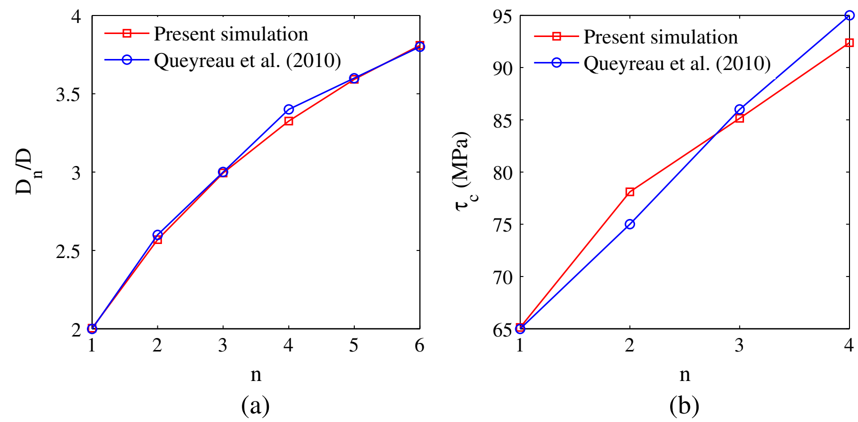

Fig. 5. (a) The diameter of n-th loop and (b) the hardening stress due to forming n loops [36].

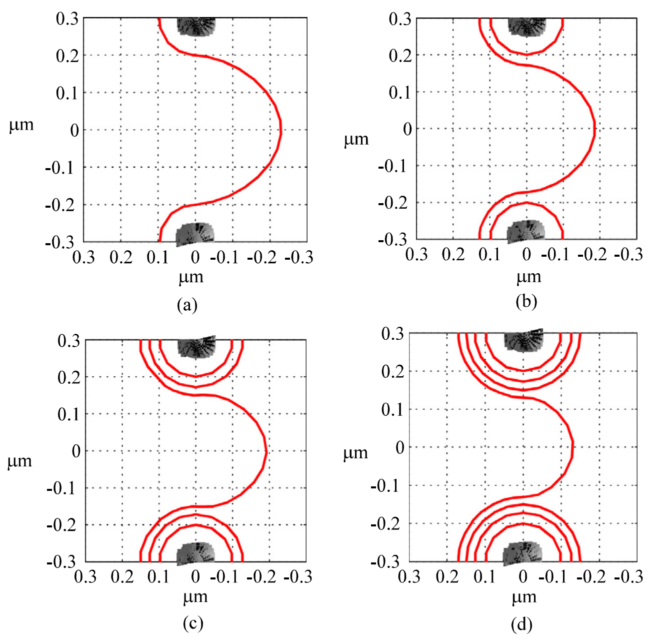

Fig. 6. The geometry of dislocation lines at the critical state: (a) $n = 1$, (b) $n = 2$, (c) $n = 3$, (d) $n = 4$.

3.3. Multi-scale analysis of plasticity in a precipitate contained micro copper cuboid

The plastic deformation in a micro copper cuboid is simulated within a multi-scale framework for various precipitate distributions. In this framework, the dislocation dynamics is adopted to model dislocation motions at the micro scale and the finite element analysis is implemented to handle the macro deformation of the cuboid. The linking of the dislocation dynamics approach to the finite element analysis is conducted through the following equation [37,38],

$$\mathbf{KU} = \mathbf{f}_{\mathbf{ext}} + \mathbf{f}_{\mathbf{B}} + \mathbf{f}_{\infty} + \mathbf{f}_{\mathbf{P}} \tag{12}$$

where $\mathbf{K}$ and $\mathbf{U}$ are the stiffness matrix and the nodal displacement vector, respectively. $\mathbf{f}_{\mathbf{ext}}$ is the applied force vector and the other terms on the right hand side are the force vectors related to the line dislocation dynamics method. The force vector, $\mathbf{f}_{\mathbf{B}}$, arises from the dislocation long range stress field and $\mathbf{f}_{\infty}$ is applied to treat boundary conditions as the dislocation stress field is usually considered in an infinite domain. The term $\mathbf{f}_{\infty}$ can be omitted if the effect of boundaries on the stress field of dislocations is considered in calculating the force vector $\mathbf{f}_{\mathbf{B}}$ [39,40]. $\mathbf{f}_{\mathbf{p}}$ arises form dislocation motions and results in the equivalent plastic strain at the finite element analysis,

$$\begin{aligned}
\mathbf{f}_{\mathbf{ext}} &= \int_{\Gamma} \bar{\mathbf{t}}\mathbf{N}\, d\Gamma \\
\mathbf{f}_{\mathbf{B}} &= \int_{\Omega} \mathbf{S}_{\mathbf{D}}\mathbf{B}\, d\Omega \\
\mathbf{f}_{\infty} &= -\int_{\Gamma} \mathbf{t}^{\infty}\mathbf{B}\, d\Gamma \\
\mathbf{f}_{\mathbf{p}} &= \int_{\Omega} \mathbf{D}\varepsilon_{\mathbf{p}}\mathbf{B}\, d\Omega
\end{aligned} \tag{13}$$

in which $\bar{\mathbf{t}}$ and $\mathbf{t}^{\infty}$ are the applied traction and the resulting traction from the presence of dislocations on the boundary Γ, respectively. $\mathbf{S}_{\mathbf{D}}$ is the average stress field due to the presence of dislocations in the finite domain, Ω, which is identical to each element at the finite element analysis. $\mathbf{N}$ is the vector of shape functions, $\mathbf{B} = \nabla\mathbf{N}$. $\varepsilon^{\mathbf{p}}$ is the plastic strain vector resulting from dislocation motions, and $\mathbf{D}$ is the elastic stiffness tensor.

Eq. (12) is solved by assuming small deformation for a cuboid copper specimen with $1 \times 1 \times 2\,\mu m$ dimensions and the same material properties of copper in Section 2. The model contains four Frank–Read sources on $(1\,1\,1)$ and $(1\ 1\ \bar{1})$ glide planes. The cuboid is discretized by $10 \times 10 \times 20$ ordinary 8-node cubic finite elements. As mentioned earlier, the generated mesh is not required to be consistent with the precipitate geometry since the developed methodology is independent from the continuum modeling, as depicted in Fig. 7. A displacement rate of $10^8\,\mu m/s$ is applied on the upper surface in the $[0\,0\,1]$ direction while the bottom surface is fixed, and the free surface condition is applied on the other four surfaces by the term $\mathbf{f}_{\infty}$ in Eq. (12). Simulations are performed for five cases: (1) precipitates are not considered; (2) the precipitates

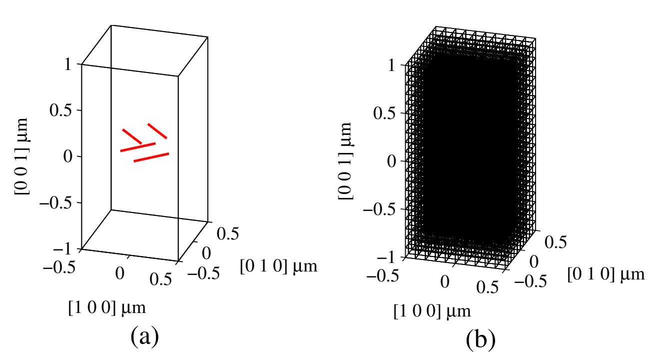

Fig. 7. (a) The initial geometry of Frank–Read sources within the cuboid and (b) the cuboid is meshed with $10 \times 10 \times 20$ ordinary 8-node cubic elements (independent from the precipitates geometry).

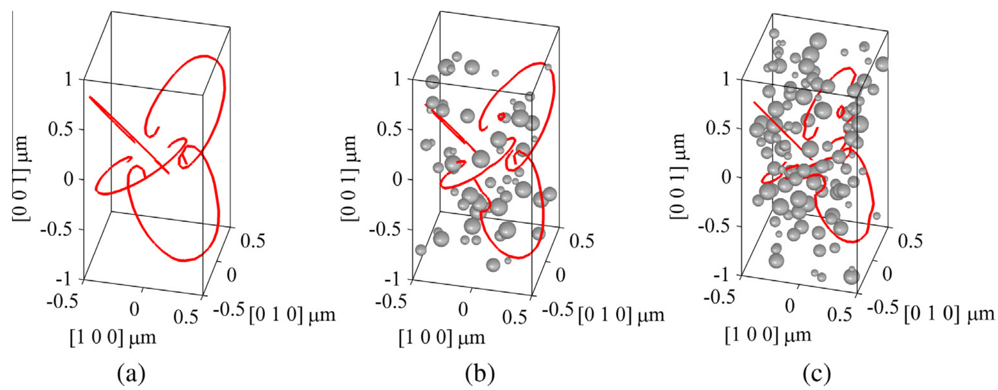

Fig. 8. The geometry of dislocations: (a) no precipitate, (b) ρ = 2% and D = 100–300 nm and (c) ρ = 4% and D = 100–300 nm.

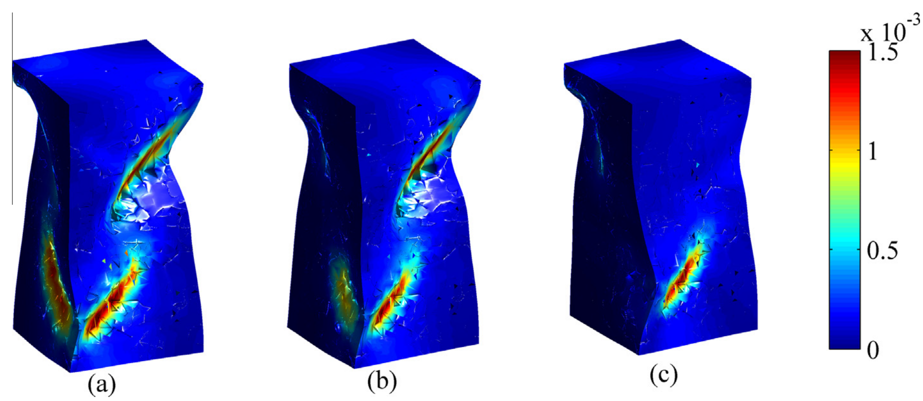

Fig. 9. The plastic deformation, exaggerated by factor 200, and the effective plastic strain: (a) no precipitate, (b) ρ = 2% and D = 100–300 nm and (c) ρ = 4% and D = 100–300 nm.

density, ρ, and the diameter of precipitates, D, are 2% and 200 nm, respectively; (3) ρ is 2%, similar to case (2), however, D varies from 100 nm to 300 nm with the average of 200 nm; cases (4) and (5) are similar to (2) and (3), respectively, while simulations are performed for the precipitates density of 4%.

The geometry of Frank–Read sources for cases (1), (3) and (5) are shown in Fig. 8. According to this figure, higher density of precipitates leads to less dislocation movements as the chance of encountering a dislocation line with precipitates increases. Fig. 9 depicts the corresponding plastic deformation for the presented cases in Fig. 8, which illustrates that a material with a higher density of precipitates responds in a more brittle behavior since the contribution of each dislocation movement to the overall macroscopic plastic deformation decreases. Fig. 10 illustrates the effective plastic strain over the whole cuboid domain and it shows that the effective plastic strain of the material decreases by increasing the precipitate content, which is in agreement with the results shown in Fig. 9.

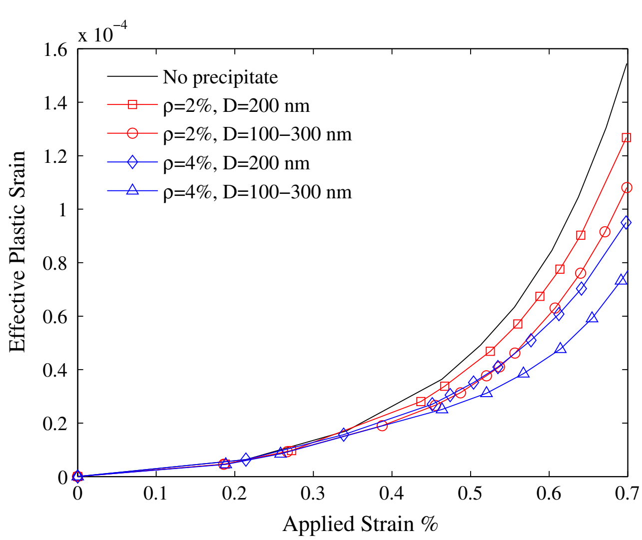

Fig. 10. The effective plastic strain versus applied strain.

4. Conclusions

A computational technique to model shearable and non-shearable precipitates within the line dislocation dynamics has been presented. The advantage of this methodology is to avoid any additional auxiliary numerical methods such as FEM, BEM or FFT since this technique stands on locking and unlocking dislocation nodes. In the present methodology, shearable precipitates are modeled by defining the resistance function for each precipitate in a way that the precipitate is cut when the exerting shear stress on the precipitate overcomes the precipitate resistance. A general form for precipitate resistance function has been proposed according to the physics of the phenomenon. In addition, non-shearable precipitates are modeled by drawing a comparison between the Frank–Read critical stress and the Orowan stress, which leads to definition of the modeling diameter parameter.

Moreover, the computational efficiency of the present methodology has been examined by implementing the technique in a combined FEM-DD framework to model the plasticity in a multi-scale framework. No mesh consistency with the geometry of precipitates is required, which reduces DOFs and the computational cost.

References

[1] L.M. Brown, R.K. Ham, Dislocation–particle interactions, Strengthening Methods in Crystals, Applied Science Publishers, London, 1971, pp. 9–135.
[2] A.J. Ardell, Precipitation hardening, Metall. Trans. A 16 (12) (1985) 2131–2165.
[3] R.J. Amodeo, N.M. Ghoniem, Dislocation dynamics. I. A proposed methodology for deformation micromechanics, Phys. Rev. B 41 (10) (1990) 6958.
[4] R.J. Amodeo, N.M. Ghoniem, Dislocation dynamics. II. Applications to the formation of persistent slip bands, planar arrays, and dislocation cells, Phys. Rev. B 41 (10) (1990) 6968.
[5] A.N. Gulluoglu, C.S. Hartley, Simulation of dislocation microstructures in two dimensions. I. Relaxed structures, Modell. Simul. Mater. Sci. Eng. 1 (1) (1992) 17.
[6] A.N. Gulluoglu, C.S. Hartley, Simulation of dislocation microstructures in two dimensions. II. Dynamic and relaxed structures, Modell. Simul. Mater. Sci. Eng. 1 (4) (1993) 383.
[7] L.P. Kubin, G. Canova, The modelling of dislocation patterns, Scr. Metall. Mater. 27 (8) (1992) 957–962.
[8] Z. Li, C. Hou, M. Huang, C. Ouyang, Strengthening mechanism in micro-polycrystals with penetrable grain boundaries by discrete dislocation dynamics simulation and Hall–Petch effect, Comput. Mater. Sci. 46 (4) (2009) 1124–1134.
[9] H. Yang, Z. Li, M. Huang, Modeling dislocation cutting the precipitate in nickel-based single crystal superalloy via the discrete dislocation dynamics with SISF dissociation scheme, Comput. Mater. Sci. 75 (2013) 52–59.
[10] R.N. Yellakara, Z. Wang, A three-dimensional dislocation dynamics study of the effects of grain size and shape on strengthening behavior of fcc Cu, Comput. Mater. Sci. 87 (2014) 253–259.
[11] H.M. Zbib, Advances in discrete dislocations dynamics and multiscale modeling, J. Eng. Mater. Technol. 131 (2009). 041209-1.
[12] M. Huang, L. Zhao, J. Tong, Discrete dislocation dynamics modelling of mechanical deformation of nickel-based single crystal superalloys, Int. J. Plast 28 (1) (2012) 141–158.
[13] T.A. Khraishi, L. Yan, Y.L. Shen, Dynamic simulations of the interaction between dislocations and dilute particle concentrations in metal–matrix composites (MMCs), Int. J. Plast 20 (6) (2004) 1039–1057.
[14] V. Mohles, Simulations of dislocation glide in overaged precipitation-hardened crystals, Philos. Mag. A 81 (4) (2001) 971–990.
[15] V. Mohles, The critical resolved shear stress of single crystals with long-range ordered precipitates calculated by dislocation dynamics simulations, Mater. Sci. Eng. A 365 (1) (2004) 144–150.
[16] V. Mohles, D. Rönnpagel, E. Nembach, Simulation of dislocation glide in precipitation hardened materials, Comput. Mater. Sci. 16 (1–4) (1999) 144–150.
[17] Y. Xiang, L.T. Cheng, D.J. Srolovitz, A level set method for dislocation dynamics, Acta Mater. 51 (18) (2003) 5499–5518.
[18] Y. Xiang, D.J. Srolovitz, L.T. Cheng, Level set simulations of dislocation–particle bypass mechanisms, Acta Mater. 52 (7) (2004) 1745–1760.
[19] C.S. Shin, M.C. Fivel, M. Verdier, K.H. Oh, Dislocation–impenetrable precipitate interaction: a three-dimensional discrete dislocation dynamics analysis, Phil. Mag. 83 (31–34) (2003) 3691–3704.
[20] A. Takahashi, N.M. Ghoniem, A computational method for dislocation–precipitate interaction, J. Mech. Phys. Solids 56 (4) (2008) 1534–1553.
[21] K. Yashiro, F. Kurose, Y. Nakashima, K. Kubo, Y. Tomita, H.M. Zbib, Discrete dislocation dynamics simulation of cutting of γ' precipitate and interfacial dislocation network in Ni-based superalloys, Int. J. Plast 22 (4) (2006) 713–723.
[22] A. Vattré, B. Devincre, A. Roos, Orientation dependence of plastic deformation in nickel-based single crystal superalloys: discrete–continuous model simulations, Acta Mater. 58 (6) (2010) 1938–1951.
[23] S. Gao, M. Fivel, A. Ma, A. Hartmaier, Influence of misfit stresses on dislocation glide in single crystal superalloys: a three-dimensional discrete dislocation dynamics study, J. Mech. Phys. Solids 76 (2015) 276–290.
[24] W. Cai, J. Deng, K. Kang, A Short Course on DDLab and ParaDiS, 2005.
[25] V.V. Bulatov, W. Cai, Computer Simulations of Dislocations, vol. 3, Springer, 2006.
[26] G. de Wit, J.S. Koehler, Interaction of dislocations with an applied stress in anisotropic crystals, Phys. Rev. 116 (5) (1959) 1113–1120.
[27] L.M. Brown, The self-stress of dislocations and the shape of extended nodes, Phil. Mag. 10 (105) (1964) 441–466.
[28] A.J.E. Foreman, The bowing of a dislocation segment, Phil. Mag. 15 (137) (1967) 1011–1021.
[29] E. Nembach, Precipitation hardening caused by a difference in shear modulus between particle and matrix, Phys. Status Solidi (a) 78 (2) (1983) 571–581.
[30] A.J.E. Foreman, M.J. Makin, Dislocation movement through random arrays of obstacles, Phil. Mag. 14 (131) (1966) 911–924.
[31] A. de Vaucorbeil, W.J. Poole, C.W. Sinclair, The superposition of strengthening contributions in engineering alloys, Mater. Sci. Eng. A 582 (2013) 147–154.
[32] A. de Vaucorbeil, C.W. Sinclair, W.J. Poole, Dislocation glide through non-randomly distributed point obstacles, Phil. Mag. 93 (27) (2013) 3664–3679.
[33] J.D. Atkinson, L.M. Brown, W.M. Stobbs, The work-hardening of copper-silica: IV. The Bauschinger effect and plastic relaxation, Phil. Mag. 30 (6) (1974) 1247–1280.
[34] L.M. Brown, W.M. Stobbs, The work-hardening of copper-silica, Phil. Mag. 23 (185) (1971) 1201–1233.
[35] J.C. Fisher, E.W. Hart, R.H. Pry, The hardening of metal crystals by precipitate particles, Acta Metall. 1 (3) (1953) 336–339.
[36] S. Queyreau, G. Monnet, B. Devincre, Orowan strengthening and forest hardening superposition examined by dislocation dynamics simulations, Acta Mater. 58 (17) (2010) 5586–5595.
[37] E. Van der Giessen, A. Needleman, Discrete dislocation plasticity: a simple planar model, Modell. Simul. Mater. Sci. Eng. 3 (5) (1995) 689.
[38] H.M. Zbib, T. Diaz de la Rubia, A multiscale model of plasticity, Int. J. Plast 18 (9) (2002) 1133–1163.
[39] Z.L. Liu, X.M. Liu, Z. Zhuang, X.C. You, A multi-scale computational model of crystal plasticity at submicron-to-nanometer scales, Int. J. Plast 25 (8) (2009) 1436–1455.
[40] M. Huang, Z. Li, Coupled DDD–FEM modeling on the mechanical behavior of microlayered metallic multilayer film at elevated temperature, J. Mech. Phys. Solids 85 (2015) 74–97.